Theoretical *versus* Experimental Charge and Spin-density Distributions in *trans*-$[Ni(NH_3)_4(NO_2)_2]$

Graham S. Chandler, Robert J. Deeth,*† Brian N. Figgis, and Robin A. Phillips
School of Chemistry, University of Western Australia, Nedlands, WA 6009, Australia

The experimental charge and spin-density distributions for $[Ni(NH_3)_4(NO_2)_2]$ have been compared with theory at various levels. *Ab initio* unrestricted Hartree–Fock (UHF) and discrete variational Xα (DVXα) Hartree–Fock–Slater molecular orbital (m.o.) calculations are reported together with cellular ligand field (c.l.f.) results. The UHF and DVXα approaches yield closely similar descriptions of the charge and spin densities, and qualitatively reproduce the main features of both types of experimental data, namely the Ni–N covalence is strong, the NO_2^- ion is a better σ donor than the NH_3 molecule, and the Ni–N π-bonding is small. Both theories indicate quite appreciable $O(NO_2)$ participation in the bonding and antibonding m.o.s involving nickel. C.l.f. calculations which include only the Ni–N interactions reproduce the experimental *d–d* spectra and the signs of the single-crystal paramagnetic anisotropies quite well, but assign a weaker σ-donor role to the nitrite ligand relative to NH_3. An extension of the model to include explicit Ni–O interactions is more satisfactory and places the NO_2^- ion as the stronger σ donor consistent with the other theoretical and experimental data.

The nature of metal–ligand bonding in transition-metal complexes can be inferred from a detailed knowledge of the molecular electron distribution.[1] The charge density corresponding to this distribution can be obtained from theory as the square of an appropriate wavefunction, and from experiment by accurate *X*-ray diffraction measurements and appropriate analysis. Ideally, the two approaches should yield the same description of the chemical bonding. In practice, agreement between experiment and theory is often only qualitative or, at best, semiquantitative.[2]

Direct comparisons between theoretical and experimental charge densities provide exacting tests of each procedure but are difficult for several reasons. First, the bonding involves essentially the valence electrons. The valence electron density is hard to evaluate from experiment because the total charge density is dominated by core electron contributions. Secondly, the *X*-ray experiment measures 'dynamic' densities since the atoms in crystals are subject to thermal vibrations. In contrast, theoretical densities are 'static.' Correction for thermal smearing is therefore required before a direct comparison can be made. These thermal effects are minimised, however, by using low temperatures. Thirdly, the usual single-determinant Hartree–Fock (HF) theory is inappropriate if electron-correlation effects are important. The far more difficult configuration interaction (c.i.) approach is then called for, although a complete treatment of as large a system as $[Ni(NH_3)_4(NO_2)_2]$ would probably be beyond the scope of present c.i. methods.[3] Finally, the experiment relates to a regular array of molecules in a crystalline lattice while calculations are usually performed on isolated units or, perhaps, on molecules embedded in a Madelung potential. The latter attempts to correct for the electrostatic effects of surrounding ions. Neither of these approaches models the real crystalline environment particularly well, especially at the periphery of the complex.[4–6]

For paramagnetic transition-metal systems the problem of dominant core contributions is avoided in the complementary technique of polarised neutron diffraction (p.n.d.). Only the unpaired electrons contribute to the experimental flipping ratios and since these electrons reside in valence-shell orbitals a picture of the valence spin density can be obtained.[7] In conjunction with detailed *X*-ray diffraction measurements, p.n.d. data provide a powerful method for probing the nature of metal–ligand bonding. Unfortunately, it is seldom possible to collect sufficient p.n.d. data to generate an accurate Fourier-transform map of the spin density. Model-based least-squares fitting procedures are therefore employed to extract useful chemical information from the experimental data and to facilitate thermal-motion corrections. The results[1] from such treatments are model dependent, although with a reasonably extensive data set all likely models can be investigated. In this way, p.n.d. has been used successfully to account for the spin density and bonding in a variety of transition-metal complexes.[8–13]

These p.n.d. studies have shown that the spin density is concentrated in the transition-metal *d* orbitals. The *d* functions and their approximate occupations are largely as expected from crystal-field theory (c.f.t.) arguments, although significant deviations from those simple predictions are usually found. The presence of spin density in ligand and formally unoccupied metal orbitals is apparent,[13] arising from two mechanisms, direct covalency and spin polarisation. The former leads to spin-density features of the same sign as the majority spin (α, positive or 'up' spin) while the latter an electron-correlation effect peculiar to paramagnetic species, may lead to spin density of the opposite sign (β, negative or 'down'). If an unpaired electron on atom A has α spin, say, then the pair of orbitals (α and β spin) in each bond to A are polarised such that the α-spin orbital increases in the vicinity of the major unpaired electron density while the β-spin orbital decreases in this region to appear elsewhere. The radial functions of the α and β orbitals are, in general, different, giving a concentration of positive (α) spin nearer the metal nucleus with concomitant negative (β) spin accumulating farther out.

Both covalency and spin polarisation are important in transition-metal complexes. Even for simple systems such as

† *Present address:* School of Chemistry, University of Bath, Claverton Down, Bath BA2 7AY.

Non-S.I. units employed: eV ≈ 1.60×10^{-19} J, a.u. ≈ 5.29×10^{-11} m, hartree ≈ 4.36×10^{-18} J.

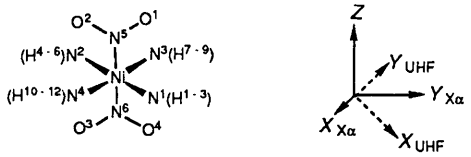

Figure 1. Geometry, axis-frame definitions, and atom labels for $[Ni(NH_3)_4(NO_2)_2]$ as used in DVXα and UHF calculations. Atoms H^1, H^4, H^7, and H^{10} lie in the *xy* plane

the $[CoCl_4]^{2-}$,[8] $[CrF_6]^{3-}$,[10] and $[Cr(CN)_6]^{3-}$ [13] ions, the apparent observation of regions of negative spin density provides experimental evidence for spin polarisation. In the cyanide complex [13] the two effects were of about the same size.

Spin-restricted theory must predict positive spin everywhere and cannot treat spin-polarisation effects.[4] A spin-unrestricted formalism is therefore a minimum requirement for attempting any theoretical comparison witn p.n.d. data. Recent unrestricted Hartree–Fock (UHF) calculations on $[CoCl_4]^{2-}$,[14] $[CrF_6]^{3-}$,[15] and *trans*-$[Ni(NH_3)_4(NO_2)_2]$ [16] have indeed shown reasonable qualitative agreement with experimental spin and charge densities. However, even for these relatively simple complexes, UHF calculations are long and extensions to larger systems with many more atoms where, for example, the surrounding lattice is included explicitly, are computationally prohibitive.

In contrast, a spin-unrestricted local-density Hartree–Fock–Slater (HFS) study,[17] using the discrete variational Xα (DVXα) formalism,[18] of the highly symmetric complex ions $[CoCl_4]^{2-}$, $[CoBr_4]^{2-}$, $[FeCl_4]^{-}$, $[CrF_6]^{3-}$, and $[Cr(CN)_6]^{3-}$ not only gave better agreement with experimental spin densities than UHF theory, but also was sufficiently fast to suggest that much larger calculations would be practical. As a step in that direction, DVXα calculations for the more complicated, mixed-ligand complex *trans*-$[Ni(NH_3)_4(NO_2)_2]$ are reported here. Both p.n.d.[19] and high-quality *X*-ray diffraction studies[20] on $[Ni(NH_3)_4(NO_2)_2]$ are available. Agreement between the DVXα results and experimental spin and charge densities is found to be good. The DVXα results also compare favourably with those of the UHF treatment and we take this opportunity to describe the UHF results in greater detail.

The complex $[Ni(NH_3)_4(NO_2)_2]$ has also stimulated a great deal of interest from a ligand-field theory (l.f.t.) point of view. In addition to experimental studies of the single-crystal polarised electronic spectra,[21,22] powder magnetic susceptibilities,[23,24] and single-crystal magnetic anisotropies,[25] several angular overlap model (a.o.m.) treatments of $[Ni(NH_3)_4(NO_2)_2]$ and related complexes have been reported.[22–24,26] However, it is now known [27] that the optical absorption observed at *ca.* 20 000 cm^{-1} is a nitrite intraligand transition and not a *d–d* band as originally assigned. Moreover, the a.o.m. studies have assumed a cylindrically symmetric Ni–NO_2 linkage, apparently for reasons of computational convenience rather than in recognition of the actual non-cylindrical symmetry of the Ni–NO_2 bond. No attempt has yet been made to account theoretically for the magnetic anisotropies in detail. These data prove to be crucial to a detailed l.f.t. analysis.

The ligand-field properties of $[Ni(NH_3)_4(NO_2)_2]$ have been re-examined here within the cellular ligand field (c.l.f.) framework of Gerloch *et al.*[28] No idealisations of the symmetry of the M–L bonds were made. The c.l.f. analysis is then compared with the description of the metal–ligand bonding derived from the UHF and DVXα molecular orbital (m.o.) calculations and the diffraction studies. The main aim of this paper is to provide a coherent picture of the electronic structure and bonding in $[Ni(NH_3)_4(NO_2)_2]$ which is, as far as possible, consistent with *all* the available theoretical and experimental data. To achieve this, it is necessary to include in the c.l.f. treatment an explicit interaction between the Ni atom and the nitrite oxygen lone-pair electrons. This appears to be the first demonstration of the importance of the role played by the oxygen atoms in N-bonded nitrite co-ordination.

Table 1. Idealised (D_{2h}) bond lengths (a.u.) and angles (°) for $[Ni(NH_3)_4(NO_2)_2]$

	Bond lengths			Bond angles	
Atoms*	UHF	DVXα	Atoms*	UHF	DVXα
Ni–NO_2	4.033	4.033	H_3N–Ni–NH_3	90.0	90.0
Ni–NH_3	3.970	3.970	Ni–N–O	121.5	121.5
N–O	2.367	2.367	O–N–O	117.0	117.0
N–H(1)	1.882	1.890	Ni–N–H(1)	114.2	112.0
N–H(2)	1.937	1.890	Ni–N–H(2)	110.4	112.0
N–H(3)	1.937	1.890	Ni–N–H(3)	110.4	112.0

* See Figure 1 for atom labels in parentheses.

Computational Details

Three different theoretical models were employed to examine the electronic structure and bonding in $[Ni(NH_3)_4(NO_2)_2]$. The details of each approach are described in turn before making a comparison of all the theoretical and experimental results.

UHF Calculations.—*X*-Ray [24] and neutron [29] diffraction studies have shown that crystals of *trans*-$[Ni(NH_3)_4(NO_2)_2]$ are monoclinic, space group $C2/m$, with $Z = 2$. Although the crystallographic site symmetry at the nickel atom is only C_{2v}, it is close to D_{2h} and the UHF calculations used this higher symmetry. However, the N–H distances and Ni–N–H angles for the hydrogens lying out of the equatorial $Ni(NH_3)_4$ plane were averaged and the H_3N–Ni–NH_3 angles were set to 90°. The nitrite N–O bond lengths were also averaged. The molecular geometry, UHF co-ordinate system, and atom numbering system are shown in Figure 1. Bond distances and angles are given in Table 1.

The co-ordinate system chosen for the UHF calculation does not coincide with the crystallographic symmetry in that the *x* and *y* axes are aligned along the Ni–NH_3 directions rather than parallel and perpendicular to the Ni–NO_2 mirror plane. Thus, the d_{z^2} and d_{xy} orbitals each transform as a_g, $d_{x^2-y^2}$ as b_{1g}, and the linear combinations $1/\sqrt{2}(d_{xz} + d_{yz})$, $1/\sqrt{2}(d_{xz} - d_{yz})$ as b_{2g} and b_{3g} respectively. In D_{2h} symmetry the 114-electron $[Ni(NH_3)_4(NO_2)_2]$ molecule has a $^3B_{1g}$ ground state from a valence electronic configuration of $14a_g^2 9b_{1u}^2 5b_{1g}^2 2a_u^2 6b_{2g}^2 {}^3b_{3g}^2 7b_{2u}^2 10b_{3u}^2 15a_g^1 6b_{1g}^1$.

The PHANTOM suite of programs [30] limited us to 256 primitive Gaussian functions. Hence, it was not possible to employ a complete double-zeta basis on all the atoms. Since the spin density is concentrated on the central nickel, this atom and its immediately bonded nitrogen atoms were given comparable basis sets (marginally better than double zeta) while the satellite oxygen and hydrogen atoms had minimal basis sets.

On the nickel atom, the primitive basis of Roos *et al.*[31] was used because it is smaller than the Wachters set.[32] The Roos basis has been studied by Hood *et al.*[33] and their prescriptions were used here. The most diffuse *s* function was deleted and the remainder contracted to double-zeta level. The *p* functions were also contracted to double-zeta level and a diffuse function ($\alpha = 0.375$) was added using the 'even tempered' criterion of Rudenberg *et al.*[34] The *d* functions were contracted without the addition of diffuse functions, giving an $(11s7p4d)/[8s5p2d]$ basis. The nitrogen basis was a $[4s2p]$ contraction of the $(8s4p)$ primitive set of van Diujneveldt,[35] as recommended by Roos

Table 2. UHF valence m.o. energies (eV) for $[Ni(NH_3)_4(NO_2)_2]$

α-Spin		β-Spin	
M.o.	Energy	M.o.	Energy
$2a_u$	−6.6063	$2a_u$	−6.6063
$6b_{1g}$	−6.6553	$5b_{1g}$	−6.6553
$15a_g$	−6.8865	$14a_g$	−7.3709
$9b_{1u}$	−7.2632	$9b_{1u}$	−7.4878
$2b_{2g}$	−8.1164	$2b_{2g}$	−8.1137
$10b_{3u}$	−8.1409	$10b_{3u}$	−8.1409
$5b_{1g}$	−12.9568		
$14a_g$	−13.9037		
$9b_{3u}$	−14.0615	$9b_{3u}$	−14.0098
$5b_{2g}$	−14.0887	$5b_{2g}$	−13.9581
$3b_{3g}$	−14.1594	$3b_{3g}$	−13.8955
$7b_{2u}$	−14.1948	$7b_{2u}$	−14.1132

et al.[31] for use with their nickel basis. For oxygen and hydrogen, the (5*s*2*p*) and (3*s*) sets of van Diujneveldt[35] were contracted to [2*s*1*p*] and [1*s*] respectively.

DVXα Calculations.—The discrete variational Xα method[18] is a numerical variant of the Hartree–Fock–Slater (HFS) local-density scheme.[36] The theory and application of the model have been described in detail elsewhere.[17,37,38] The matrix elements of the secular equation are approximated numerically by a weighted summation over a grid of sample points. These points are distributed pseudo-randomly via a Diophantine procedure and the desired level of accuracy can be achieved simply by using a sufficiently large number of points.

Calculations within the spin-unrestricted DVXα formalism were carried out on $[Ni(NH_3)_4(NO_2)_2]$. Spin-restricted DVXα results were also obtained for the isolated closed-shell molecules NH_3 and NO_2^-. As for the UHF calculations, the point symmetry was idealised to D_{2h} but with *x* perpendicular to the mirror plane (*i.e.* *x* and *y* bisect the H_3N–Ni–NH_3 angles, d_{xy} transforms as b_{1g} and $d_{x^2-y^2}$ as a_g). Bond lengths and angles are given in Table 1. The same geometries used for the complex were also employed for the calculations on the isolated ligands. Note that all the N–H distances were assigned the same values, as were all the H–N–H angles. Optimised atomic orbital (a.o.) basis sets up to 4*p* on Ni, 2*p* on N and O, and 1*s* on H were employed. Potential wells were applied to each basis set to confine diffuse orbitals to reasonable molecular proportions. Such basis sets have been shown to be of approximately double-zeta quality.[39] The self-consistent charge (s.c.c.) scheme[40] was employed since it speeds up the calculation considerably without severely affecting the accuracy. The s.c.c. procedure also provides a convenient measure of the self-consistent field convergence. A total of 3 000 sampling points were used for the complex. For the isolated ligands NH_3 and NO_2^-, 600 and 750 points respectively were employed to maintain a consistent level of accuracy. A numerical error of approximately 0.06 eV in m.o. energies, 0.03 in orbital charge populations, and 0.003 in spin populations is anticipated with this sampling scheme. The scaling parameter, α, for the HFS exchange/correlation operator was fixed at 0.7 throughout. This value has been found to give accurate results for a wide variety of different molecules and molecular properties.[37,38]

C.L.F. Calculations.—Ligand-field calculations were carried out within the c.l.f. framework.[28,41] The c.l.f. model is synonymous with the ligand-field version of the a.o.m. No symmetry idealisations are required and the observed atomic co-ordinates[19] were employed. As with the DVXα calculations, the global cartesian axes reflect the crystal site symmetry with *z* along the Ni–NO_2 vector and *x* perpendicular to the NO_2 plane. The c.l.f. model parametrises metal–ligand interactions in terms of the local M–L pseudo-symmetry.[28] This scheme leads naturally to a separation of the M–L interaction into σ and π components.

The σ-bonding parameters $e_\sigma(NH_3)$ and $e_\sigma(NO_2)$, are directed along the appropriate M–L vectors, while the π interactions perpendicular to these directions are treated *via* the e_π parameters. The π bonds are also defined with respect to the local symmetry. For NO_2^- there are two obvious π-bonding directions, one perpendicular to the ligand plane $[e_{\pi\perp}(NO_2)]$ and one parallel to the ligand plane $[e_{\pi\parallel}(NO_2)]$. All the in-plane *p*-orbitals on the nitrite N atom are involved in hybrids which form σ bonds with the O atoms or else contain the lone pair. Consequently, what would be the $N_{\pi\parallel}$ orbitals are deemed to be unavailable for Ni–NO_2 co-ordination and $e_{\pi\parallel}(NO_2)$ is set equal to zero. Similarly, there are no accessible π functions for ammonia and $e_\pi(NH_3)$ is also set to zero. The three c.l.f. parameters $e_\sigma(NH_3)$, $e_\sigma(NO_2)$, and $e_{\pi\perp}(NO_2)$ (scheme CLF1) are used in conjunction with the Racah interelectron repulsion parameter, *B*, the one-electron spin–orbit coupling constant, ζ, and Steven's orbital reduction factor, *k*. All the calculations were performed within the complete spin-triplet d^8 basis, comprising the ^3F and ^3P free-ion terms, using the CAMMAG suite of programs.[42]

During the course of this work it became apparent that scheme CLF1 was inadequate. A second parameter set, scheme CLF2, was therefore devised. This scheme incorporated an explicit Ni–O interaction in the form of a single c.l.f. parameter, $e_\sigma(O)$, directed along the Ni–O vector. Further investigations of this parameter were made by calculating the *d*–*d* spectrum of the $[Ni(NO_2)_6]^{4-}$ ion, using atomic co-ordinates taken from ref. 43. The parameter set comprised $e_\sigma(NO_2)$, $e_{\pi\perp}(NO_2)$, $e_\sigma(O)$, and *B*. Since magnetic properties were not required, both ζ and *k* were set to zero.

Results and Discussion

UHF Orbital Energies.—The UHF valence orbital energies, with the unpaired electrons having α spin, are given in Table 2. The total energy was −2 136.5784 hartree and $\langle S^2 \rangle$ = 2.0023, indicating that spin contamination is negligible.

The ordering of levels in Table 2 may appear unconventional in that the $6b_{1g}(\alpha)$ and $15a_g(\alpha)$ m.o.s have been paired with the $5b_{1g}(\beta)$ and $14a_g(\beta)$ orbitals. This emphasises that most of the unpaired spin resides in the $5b_{1g}(\alpha)$ and $14a_g(\alpha)$ functions and not in the $6b_{1g}(\alpha)$ and $16a_g(\alpha)$ levels of the conventional configuration given previously. Ordered as they are in Table 2, it is clear that the α- and β-spin orbitals are matched closely in energy apart from the two containing the unpaired electrons. Examination of the wavefunctions for the $6b_{1g}(\alpha)$ and $5b_{1g}(\beta)$ m.o.s shows them to be very similar, as also are $15a_g(\alpha)$ and $14a_g(\beta)$. The former pair consist almost exclusively of oxygen $2p_x$ and $2p_y$ functions, $0.35[O1(p_x) - O2(p_x) + O3(p_x) - O4(p_x) - O1(p_y) + O2(p_y) - O3(p_y) + O4(p_y)]$, while the latter pair are mainly a nickel *s* function, diffuse enough to be classified as 4*s*, interacting with the oxygen p_z functions in an antibonding fashion. There is a lesser admixture of nitrite N p_z and *s* functions, $0.4[Ni(s) + O1(p_z) + O2(p_z) - O3(p_z) - O4(p_z) + \ldots]$.

The $5b_{1g}(\alpha)$ and $14a_g(\alpha)$ m.o.s have no β-spin counterparts. Crystal field theory places the unpaired electrons in the $d_{x^2-y^2}$ (b_{1g}) and d_{z^2} (a_g) orbitals (in the UHF axis frame, Figure 1). Consequently, the $5b_{1g}$ m.o. consists of $d_{x^2-y^2}$ functions heavily mixed with ammine nitrogen p_x and p_y functions [0.32 $d_{x^2-y^2}$ + 0.17 $d_{x^2-y^2}$ − 0.27 N3(p_y) − 0.24 N3(p_y) + 0.27 N4(p_y) + 0.24 N4(p_y) + 0.27 N1(p_x) + 0.24 N1(p_x) − 0.27 N2(p_x) − 0.24 N2(p_x)]. Similarly, the major contributions to the $14a_g$

Table 3. DVXα valence m.o. energies (eV) and a.o. compositions (%); h.o.m.o. indicated by *

(*a*) NH_3

		N		H
M.o.	Energy	2*s*	2*p*	1*s*
$4a_1$	8.519	14.5	8.9	76.6
$2e$	7.986	—	36.1	63.9
$3a_1$ *	−5.636	11.6	85.9	2.5
$1e$	−11.409	—	63.9	36.1
$2a_1$	−21.599	74.0	5.2	20.8

(*b*) NO_2

		N		O	
M.o.	Energy	2*s*	2*p*	2*s*	2*p*
$5b_1$	18.492	—	56.4	7.5	36.1
$7a_1$	18.070	21.9	29.0	7.8	41.3
$2b_2$	7.237	—	53.0	—	47.0
$6a_1$ *	4.158	8.6	17.5	0.0	73.9
$4b_1$	3.127	—	0.0	0.1	99.9
$1a_2$	2.609	—	0.0	—	100.0
$1b_2$	−1.350	—	47.0	—	53.0
$5a_1$	−1.731	3.4	44.7	3.2	48.7
$3b_1$	−2.206	—	22.3	16.3	61.4
$4a_1$	−5.547	30.9	4.9	36.6	27.6
$2b_1$	−14.381	—	21.2	76.1	2.7

m.o. are the d_{z^2} functions (0.35 d_{z^2} + 0.19 d_{z^2}) with a lesser but significant mixing of nitrogen p_x, p_y, p_z, and *s* functions and the oxygen *p* orbitals. Both singly occupied levels have ample covalent interaction to allow spin delocalisation even onto the oxygen atoms of the nitrite ions.

DVXα Valence M.O. Energies and A.O. Compositions.—The a.o. compositions of the DVXα m.o.s for NH_3 are collected in Table 3(*a*). The highest occupied molecular orbital (h.o.m.o.), $3a_1$, is almost entirely (86%) a nitrogen 2*p* function, corresponding to the lone pair of electrons. It is energetically well separated from any other orbitals, occupied or virtual, and is thus expected to provide the dominant ligand contribution to the metal–ammonia bond.

In the complex, the Ni–NH_3 bonding is concentrated in the b_{1g} m.o.s. Inspection of the m.o. compositions for $[Ni(NH_3)_4(NO_2)_2]$ (Table 4) indicates that most of the NH_3 σ bonding is described by the $4b_{1g}(\alpha,\beta)$ and $6b_{1g}(\alpha)$ orbitals in which the nitrogen lone-pair 2*p* orbitals mix with metal *d* functions. The dominance of the N 2*p* function in the ammonia part of these m.o.s is consistent with the ligand mainly using its $3a_1$ orbital for σ bonding. The similar compositions of the $4b_{1g}$ α- and β-spin orbitals mean that the spin in the *xy* plane will be described largely by the $6b_{1g}(\alpha)$ density. Since there are no energetically accessible NH_3 π functions, a vanishingly small nickel–ammonia π interaction is anticipated. In fact, the largest Ni–NH_3 π interaction occurs in the $8b_{1u}$ m.o., which is mainly nitrite based, and shows only 2% ammonia 2*p* character.

The above discussion illustrates the use of frontier molecular orbital (f.m.o.) analysis of the isolated ligands as a guide to the nature of the metal–ligand bonding in $[Ni(NH_3)_4(NO_2)_2]$. This approach has been used previously in connection with DVXα calculations on substituted ammines and phosphines.[44] The f.m.o. analysis of ammonia co-ordination is relatively straightforward. That for nitrite co-ordination is more complex. The main σ interaction focuses on the $6a_1$ orbital of the free ligand [Table 3(*b*)]. This function is comprised mainly of oxygen 2*p* orbitals lying in the nitrite plane with only a 17.5% contribution from the nitrogen $2p_z$ orbital which lies along the ligand C_2 axis. The Ni–NO_2 σ interactions in $[Ni(NH_3)_4(NO_2)_2]$ are spread over the α- and β-spin orbitals of $12a_g$, $13a_g$, and $14a_g$ symmetry plus the $15a_g(\alpha)$ function. Generally, the contribution from the oxygen atoms is substantially larger than that from the nitrogens. A similar picture emerged from the UHF calculation. The heavy involvement of oxygen in the Ni–NO_2 bond is also consistent with the ligand using its $6a_1$ f.m.o. In contrast to the Ni–NH_3 bonds, the Ni–NO_2 spin density cannot be attributed to a single function since the various α-spin m.o.s do not have similarly composed β-spin counterparts. Instead, the spin results from a cancellation by the β-spin $13a_g$ and $14a_g$ orbitals of the α-spin density contained in the $13a_g$, $14a_g$, and $15a_g$ functions.

For the free nitrite ion the valence π functions are somewhat closer to the h.o.m.o. than for ammonia. A larger π interaction with a metal atom is therefore expected. However, the $2b_2$ virtual orbital of free NO_2^-, which describes π bonding perpendicular to the ligand plane, is still over 3 eV above the h.o.m.o. In $[Ni(NH_3)_4(NO_2)_2]$ this orbital appears in m.o.s of b_{2g} and b_{3u} symmetry. The mixing between metal and nitrite orbitals for these m.o.s is small (Table 4), suggesting that the Ni–NO_2 out-of-plane π bond is very weak. In contrast, the filled in-plane orbital of the free nitrite ion is much closer to the h.o.m.o. and plays a significant role in the $6b_{3g}(\beta)$ and $5b_{3g}(\alpha)$ m.o.s of $[Ni(NH_3)_4(NO_2)_2]$. These functions are largely oxygen based. The data in Table 4 also show an overall larger ligand contribution to the Ni–NO_2 bonds than to the Ni–NH_3 linkages. Conversely, the *d*-orbital component in the a_g functions, which describe the nitrite σ bonding, is less than that in the $6b_{1g}(\alpha)$ orbital, which describes the ammonia σ bonds (75 *versus* 85%).

To summarise, the DVXα m.o. composition analysis for $[Ni(NH_3)_4(NO_2)_2]$ suggests a stronger nitrite σ interaction relative to that from ammonia. Although the bonding is formally *via* the N atom the nitrite oxygen plays a significant role. Ammonia σ bonds mainly *via* its nitrogen 2*p* orbitals and there is virtually no Ni–NH_3 π bonding. There is a small Ni–NO_2 π interaction perpendicular to the ligand plane with a larger interaction parallel to the NO_2 plane and dominated by oxygen 2*p* functions.

Charge and Spin Populations.—The metal–ligand bonding in $[Ni(NH_3)_4(NO_2)_2]$ can be examined further *via* a Mulliken analysis of the DVXα and UHF ground-state wavefunctions. Although Mulliken populations cannot be taken literally, a good qualitative picture can be constructed by comparing results for the unco-ordinated and co-ordinated ligands. The results from the two theoretical approaches and the experimentally derived spin- and charge-density data are collected in Table 5. For $[Ni(NH_3)_4(NO_2)_2]$ the DVXα and UHF populations are very similar, so that it matters little which theoretical scheme is discussed in detail. The main difference between the DVXα and UHF data is that the former predicts somewhat greater covalency and so is in slightly better agreement with the reported experimental results. The discussion of the computational results therefore centres on the DVXα data.

There is a close connection between the DVXα m.o. composition analysis of the preceding section and that based on Mulliken populations. For example, the total charge on NO_2^- decreases by 0.34 electrons on co-ordination compared to a fall of only 0.012 for NH_3. This conforms with the earlier conclusion of a stronger metal–nitrite interaction. A quantitative picture of the charge redistribution can be obtained by computing, for the ligand hybrids and the nickel orbitals, the population changes accompanying bonding.

The population in the ammonia sp^3 hybrid orbital directed at Ni decreases by about 0.15 electrons relative to the free ligand.

Table 4. DVXα valence m.o. energies (eV) and a.o. compositions (%) for $[Ni(NH_3)_4(NO_2)_2]$; h.o.m.o. is $15a_g(\alpha)$. Unoccupied and low-energy orbitals not shown

		Ni			O		$N(NH_3)$		$N(NO_2)$		H
M.o.	Energy	3*d*	4*s*	4*p*	2*s*	2*p*	2*s*	2*p*	2*s*	2*p*	1*s*
$15a_g(\alpha)$	−2.837	34.5	2.4			43.2	0.5	3.8	5.1	10.6	
$14a_g(\beta)$	−3.006	98.2									1.8
$6b_{3g}(\beta)$	−3.166	84.9				14.5					0.6
$3b_{2g}(\beta)$	−3.346	94.7				3.8				0.4	1.1
$6b_{1g}(\alpha)$	−3.559	82.8					2.8	14.0			0.4
$9b_{1u}(\beta)$	−3.621			5.4	−0.2	84.4		0.1	2.8	7.3	0.2
$6b_{3g}(\alpha)$	−3.683	1.6			0.2	98.0		0.2			
$9b_{1u}(\alpha)$	−3.714			5.6		84.7		0.1	2.6	6.9	0.1
$10b_{2u}(\beta)$	−3.714			0.3	0.2	98.8	0.2	0.2			0.3
$5b_{3g}(\beta)$	−3.723	13.8			0.1	85.6		0.4			0.1
$10b_{2u}(\alpha)$	−3.773			0.3	0.2	98.8	0.2	0.2			0.3
$13a_g(\beta)$	−4.080	22.1	3.5			71.0			0.8	2.6	
$2a_u(\beta)$	−4.449					99.8		0.2			
$5b_{1g}(\beta)$	−4.483					99.7	0.1	0.1			0.1
$2a_u(\alpha)$	−4.507					99.8		0.2			
$5b_{1g}(\alpha)$	−4.542					99.7		0.1			0.2
$14a_g(\alpha)$	−4.788	76.9	0.9			20.9	0.1	0.3			0.9
$13a_g(\alpha)$	−4.802	73.7	1.2			23.9	0.1	0.6			0.8
$5b_{3g}(\alpha)$	−5.059	96.8				2.3		0.2			0.7
$3b_{2g}(\alpha)$	−5.085	96.4				2.7					0.9
$7b_{3u}(\beta)$	−8.694			−0.8		33.6	3.4	27.8		34.7	1.3
$7b_{3u}(\alpha)$	−8.778			−0.6		33.7	3.2	27.1		35.3	1.3
$2b_{2g}(\beta)$	−8.893	0.6				44.9		1.3		52.3	0.9
$2b_{2g}(\alpha)$	−8.896	1.2				44.1		1.3		52.4	1.0
$9b_{2u}(\beta)$	−9.006			−0.4	10.3	31.4	3.8	42.2		11.3	1.4
$4b_{1g}(\beta)$	−9.031	10.6					7.4	79.2			2.8
$9b_{2u}(\alpha)$	−9.093			−0.2	10.8	32.7	3.6	39.9		11.8	1.3
$12a_g(\beta)$	−9.181	6.4	−0.5		4.8	33.4	2.4	21.5		30.5	1.1
$4b_{3g}(\beta)$	−9.246	0.3			20.9	56.3			22.4		0.1
$8b_{1u}(\beta)$	−9.298			3.8	7.6	44.9		2.2	0.4	39.8	1.2
$4b_{3g}(\alpha)$	−9.329	0.5			21.0	55.9				22.4	0.1
$4b_{1g}(\alpha)$	−9.336	16.9					6.5	73.9			2.7
$12a_g(\alpha)$	−9.396	10.2	−0.4		5.7	33.1	2.0	18.5	0.3	29.7	1.0
$8b_{1u}(\alpha)$	−9.404			4.0	7.9	44.7		2.3	0.3	39.5	1.2
$8b_{2u}(\beta)$	−9.486			−0.7	10.7	25.4	3.9	47.8		11.1	1.8
$6b_{3u}(\beta)$	−9.574			0.8		12.7	4.4	60.9		18.5	2.6
$8b_{2u}(\alpha)$	−9.577			−0.2	10.3	24.0	4.0	49.6		10.6	1.8
$6b_{3u}(\alpha)$	−9.675			1.4		12.3	4.3	61.1		18.2	2.7
$11a_g(\beta)$	−10.702	0.7	3.4		7.9	15.1	2.7	61.2	1.6	6.0	1.5
$11a_g(\alpha)$	−10.852	1.2	4.3		7.8	14.0	2.6	61.7	1.8	5.1	1.6

If this change is attributed to σ donation to the metal then there is a conflict in that the sum of the individual N and H atomic charges gives an overall change in the NH_3 charge of only 0.012. It is apparent that co-ordination results in a build-up of charge on the ammonia nitrogen atoms both from the lone-pair hybrid as well as from the H atoms. The movements of charge within the ammonia ligand are relatively large but the net transfer of charge to the nickel atom remains small.

The hybrid-orbital populations in the N–O σ framework of the nitrite ligand are almost unchanged on co-ordination. Thus, in contrast to the NH_3 case, the 0.14-electron decrease in the population of the N sp^2 hybrid directed at the metal can be attributed directly to σ donation. However, this accounts for only about half of the total nitrite charge transfer of 0.34, the remainder coming from the oxygen lone pairs. Note that despite the dominance of the oxygen-based orbitals in the m.o. compositions, the nitrogen atom is closer to the metal and so has a greater overlap and charge donation. Since the $4b_1$ orbital of the free nitrite ion is filled, the Ni–O interaction is expected to be of a donor type, consistent with the decreasing lone-pair populations on oxygen. Any out-of-plane nitrite π interaction is expected to be an acceptor type since the relevant orbital in the free ligand is vacant. The N p_π population does indeed increase by about 0.13 electrons although part of this appears to come from a polarisation of the N–O bond. The O p_π populations each decrease by 0.06 and hence there is only a 0.01 p_π increase over the whole ligand. The extent of π backbonding therefore is quite small.

The nickel-orbital populations show that the bulk of the charge donation, particularly from the nitrite groups, is accommodated in the $3d_{z^2}$, $4p_z$, and 4*s* functions. The first two orbitals are optimally oriented to accept the nitrite σ charge. Virtually all the spin is concentrated in σ-type orbitals. There is about four times as much spin transfer to NO_2^- (0.112 electrons) than to NH_3 (0.026 electrons). The H atoms have a small negative spin (−0.002) while all the nitrite in-plane orbitals adopt fairly substantial positive spin populations. The spin density perpendicular to the nitrite plane is very small, being positive on N and negative on O.

The calculated overlap populations, both charge and spin, generally support a larger Ni–NO_2 interaction, although the Ni–NO_2 spin overlap of −0.03 is only about half that calculated for the Ni–NH_3 bonds. The importance of the Ni–O interaction is manifest in a charge-overlap population of −0.06 compared to −0.09 for the Ni–NH_3 bonds.

The experimentally derived spin and charge populations are

Table 5. Calculated and experimental orbital and overlap populations for $[Ni(NH_3)_4(NO_2)_2]$ and isolated ligands NH_3 and NO_2^-

		Spin			Charge			
	Orbital	DVXα	P.n.d.[a]	UHF	DVXα	*X*-Ray[a]	UHF	Ligand DVXα
Ni	d_{xy}	0.89	0.87(7)	0.97	1.11	1.28(7)	1.04	
	d_{yz}	0.00	0.04(4)	0.00	1.99	1.80(6)	1.97	
	d_{xz}	0.02	−0.02(7)	0.00	1.94	1.31(6)	1.98	
	d_{z^2}	0.68	0.84(7)	0.94	1.31	1.36(8)	1.22	
	$d_{x^2-y^2}$	0.01	−0.05(6)	0.00	1.97	1.84(7)	1.98	
	κ_r (3*d*)[c]	1.035	0.92(1)	—	1.04	1.013(6)	—	
	$4s + 4p_x$	0.02	0.17(6)	−0.01	0.06	1.59(20)	0.12	
	$4s + 4p_y$	0.02	0.07(6)	−0.01	0.04	0.09(20)	0.12	
	$4s + 4p_z$	0.02	−0.14(7)	−0.01	0.31	−0.19(20)	0.20	
NH_3	sp^3 (N→Ni)	0.011	0.033(9)	0.019	1.64	1.59(3)		1.79
	sp^3 (N→H^1)	0.007	0.000(7)	0.019	1.57	1.24(2)	5.51	1.43
	sp^3 (N→$H^{2,3}$)	0.007	0.001(4)	0.019	1.57	1.21(3)		1.43
	1*s* (H^1)	−0.002	−0.001(8)	−0.002	0.55	0.77(4)	0.84	0.64
	1*s* (H^2, H^3)	−0.002	0.026(5)	−0.003	0.55	0.93(3)	0.82	0.64
	Ni–N_{ov}	−0.063	−0.050(11)		−0.09	−0.02		
NO_2	sp^2 (N→Ni)	0.028	0.104(20)	0.017	1.70	1.66(4)		1.47
	sp^2 (N→O)	0.012	−0.009(14)	0.017	1.17	1.29(4)	5.12	1.19
	p_π (N)	0.000	−0.008(7)	0.017	1.07	0.86(4)		0.94
	sp^2 (O→N)	0.009	0.005(14)	0.002	1.61	(1.53)[b]		1.61
	sp^2 (O→*lp*)	0.013	0.005(8)	0.002	1.69	(1.64)[b]	6.35	1.73
	p_π (O)	−0.005	0.004(8)	0.002	1.47	(1.50)[b]		1.53
	Ni–N_{ov}	−0.031	−0.067(14)		0.372		0.213	
	Ni–O_{ov}	0.003			−0.056			

[a] Estimated standard deviations for experimental data in parentheses. [b] Values converted from reported *sp* hybrid-orbital populations for individual oxygen atoms into approximate average populations. [c] Ratio of calculated and free-ion *d*-orbital radii.

broadly similar to the theoretical values. The comparison cannot be direct since the Mulliken population analysis has a different basis to the least-squares models used to analyse the experimental diffraction data. The actual numerical agreement is nevertheless quite close (Table 5) despite these differing methods. The main deviation appears to be with the diffuse metal-orbital populations. Nevertheless, the chemistry suggested by the experimental data supports the theoretical analysis. That is, NO_2^- is a stronger σ donor than NH_3, NH_3 shows no π interaction, and NO_2^- displays small π bonding perpendicular to the ligand plane but of uncertain sign (acceptor from p.n.d.[19] and donor from *X*-ray[20] diffraction).

The experimentally derived metal-orbital populations show most of the spin concentrated in the σ symmetry functions d_{z^2} and d_{xy} (DVXα axis frame, Figure 1). There is a concomitant charge build-up in these orbitals relative to the c.f.t. prediction of $d_{z^2}^1 d_{xy}^1$. The main discrepancies are the very low $3d_{xz}$ population and the very high $4p_x$ population from the *X*-ray diffraction analysis which are not reproduced theoretically. It has been suggested[20] that c.i. mixes into the ground state an excited state in which two electrons are promoted from $3d_{xz}$ to $4p_x$. This would account for the experimental observations but we defer further comment to the end of this paper.

Spin-density Maps.—The close agreement between the DVXα and UHF results for $[Ni(NH_3)_4(NO_2)_2]$ is displayed pictorially in the spin-density maps of Figure 2. Qualitatively, the DVXα model predicts greater overall spin delocalisation while the UHF approach gives greater spin polarisation. Thus, the positive peaks on the metal side of the nitrogen atoms are all about twice as high in the DVXα maps [Figure 2 (*a*) and 2(*d*)] than the UHF maps [Figure 2(*b*) and 2(*e*)], while the oxygen features are 8—16 times higher. The latter discrepancy may be due to the relatively poorer description of the oxygen atoms in the UHF study. The negative features are all deeper for the UHF spin density than for the DVXα case.

The experimental Ni–NO_2 spin density is also shown in Figure 2(*c*). The theoretical maps are broadly similar to experiment around the Ni and N atoms but, even though the lowest two or three contours of Figure 2(*c*) are below experimental error, it is apparent that the negative, spin-polarisation features found experimentally are not completely reproduced by theory. Moreover, the oxygen features appear to display a different symmetry. Whether this discrepancy is due to shortcomings in the modelling of the experimental data or to deficiencies in the theoretical methods employed is unclear at present.

Cellular Ligand Field Analysis.—The qualitative description of the Ni–N bonding in $[Ni(NH_3)_4(NO_2)_2]$ derived from diffraction experiments and from m.o. theory is the same. The m.o. calculations have also indicated a significant Ni–O interaction. A c.l.f. analysis of this system is therefore of interest not only to correct the deficiencies of previous treatments but also to examine whether the same description of the chemistry will emerge. The spectral and magnetic properties of $[Ni(NH_3)_4(NO_2)_2]$ have been measured in considerable detail.[21–26] Of particular interest here are the single-crystal polarised electronic spectra of Hare and Ballhausen[21] and the magnetic anisotropies of Figgis *et al.*[25]

Two low-energy absorptions are resolved[21] at 12 000 and 11 200 cm^{-1} corresponding to transitions from the ground state to the split components of the $^3T_{2g}$ level (labelled in O_h symmetry). A second, stronger absorption is observed around 20 000 cm^{-1} apparently split into two components at 19 900 and 20 350 cm^{-1}. The broad band system at 20 000 cm^{-1} was originally thought[21] to be '*d–d*' in origin [$^3A_{2g} \longrightarrow {}^3T_{1g}(F)$ in O_h] but it is now believed[27] to be a nitrite intraligand transition. Hence, in the present c.l.f. analysis, no significance is attached

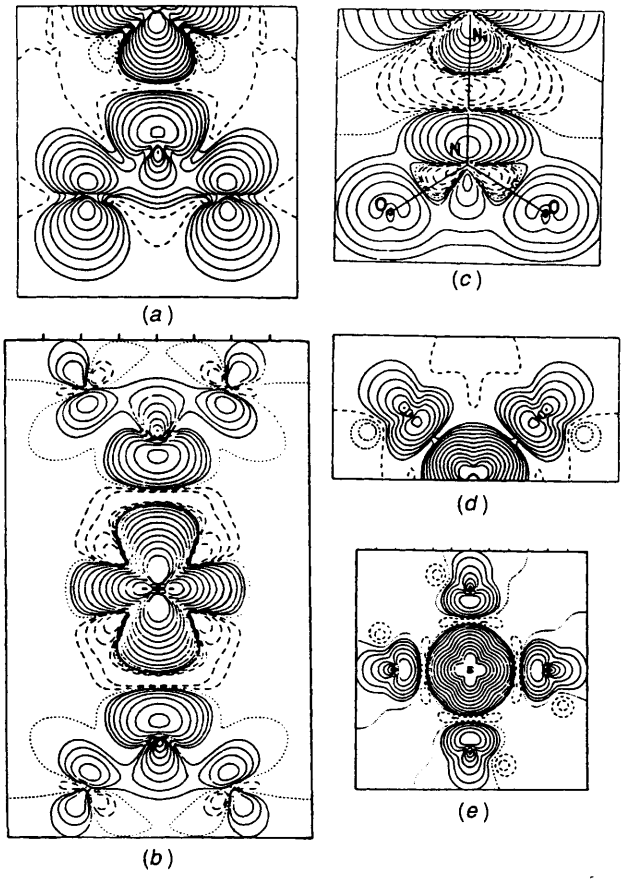

Figure 2. Theoretical and experimental spin-density plots for $[Ni(NH_3)_4(NO_2)_2]$: (*a*) DVXα in the *xz* Ni–NO_2 plane; (*b*) UHF in the *xz* Ni–NO_2 plane; (*c*) experimental (ref. 19) in the *xz* Ni–NO_2 plane; (*d*) DVXα in the *xy* $Ni(NH_3)_4$ plane; and (*e*) UHF in the *xy* $Ni(NH_3)_4$ plane. Solid lines are positive contours, dashed lines are zero or negative contours. Short dash is zero for (*b*), (*c*), and (*e*), long dash is zero for (*a*) and (*d*). Adjacent contours differ by a factor of two and the highest positive contour is 0.5 spin a.u.$^{-3}$

to the energy maximum of this band apart from requiring that the calculated components of the nominal $^3T_{1g}(F)$ level lie somewhere under the absorption envelope between, say, 17 000 and 23 000 cm^{-1}.

Since the energy difference $^3B_{1g} \longrightarrow {}^3B_{2g}$ in tetragonal nickel complexes is equal to $3e_\sigma$(eq), where eq refers to the equatorial ligands, the original assignment[21] (in D_{4h} symmetry) of the band at 12 000 cm^{-1} to this transition would fix $e_\sigma(NH_3)$ at 4 000 cm^{-1}. The lower-energy band is then the $^3B_{1g} \longrightarrow {}^3E_g$ absorption. Bertini *et al.*[22] chose to invert this assignment leading to an $e_\sigma(NH_3)$ value of 3 700 cm^{-1}. However, their own a.o.m. analysis of $[Ni(NH_3)_4(NO_2)_2]$ and related complexes, together with the more extensive treatment by Lever *et al.*,[26] suggested a linear relationship between e_σ(N) for a saturated equatorial amine and the $Ni–N_{eq}$ bond length, at least in the range 1.9—2.3 Å. The $e_\sigma(NH_3)$ value of Bertini *et al.* for $[Ni(NH_3)_4(NO_2)_2]$ lies somewhat off this correlation (see Figure 6, ref. 22). Using the original spectral assignment, an $e_\sigma(NH_3)$ value of 4 000 cm^{-1} is more consistent with the previous work and is therefore used here.

Further support for these choices comes from the nearly identical behaviour of the magnetic moments of $[Ni(NH_3)_4(NO_2)_2]$ and $[Ni(en)_2(NO_2)_2]$ (en = ethylenediamine).[23] The zero-field splitting parameters for both complexes have the same sign indicating the same sign for the splitting of the $^3T_{2g}$ (in O_h) term, *i.e.* $^3E_g < {}^3B_{2g}$ (in D_{4h}). This ordering was also

Table 6. C.l.f. parameter values for the 'best fit' (CLF1) and a representative fit (CLF2) of the spectral and magnetic data for $[Ni(NH_3)_4(NO_2)_2]$. All values in cm^{-1} except *k* (dimensionless), φ (°), and χ (c.g.s. units). Magnetic anisotropy data from ref. 25 were reorganised according to the prescriptions of ref. 41 to facilitate the CAMMAG calculations

	CLF1	CLF2	Observed
$e_\sigma(NH_3)$	4 000	4 000	
$e_\sigma(NO_2)$	3 200	4 500	
$e_{\pi\perp}(NO_2)$	−400	−800	
$e_\sigma(O)$	—	−1 200	
ζ	375	400	
B	(850)	(850)	
k	1.0	1.0	
$^3B_{1g} \longrightarrow {}^3E_g$	10 864	11 764	11 200
	11 421	11 945	
$^3B_{1g} \longrightarrow {}^3B_{2g}$	11 987	12 102	12 000
$^3B_{1g} \longrightarrow [{}^3T_{1g}(F)]$ *	17 414	17 509	20 000
	17 981	19 312	
	19 100	19 618	
$^3B_{1g} \longrightarrow [{}^3T_{1g}(P)]$ *	28 869	29 808	>25 000
	29 032	30 061	
	29 252	30 222	
$\chi_2 - \chi_3$ (300 K)	−2	−9	−16 ± 4
$\chi_2 - \chi_3$ (80 K)	−8	−31	−48 ± 15
$\chi_1 - \chi_3$ (300 K)	−43	−69	−80 ± 20
$\chi_1 - \chi_3$ (80 K)	−132	−86	−382 ± 121
$\chi_2 - \chi_1$ (300 K)	42	60	64 ± 15
$\chi_2 - \chi_1$ (80 K)	123	55	334 ± 106
φ (300 K)	−2	−1	0
φ (80 K)	−2	−1	0
$\chi_{av.}$ (300 K)	3 969	3 897	4 011 ± 40
$\chi_{av.}$ (80 K)	14 383	14 334	14 029 ± 158

* O_h term labels.

derived from the polarised spectra of the en analogue[22] and is identical to the original proposal for $[Ni(NH_3)_4(NO_2)_2]$.

The remaining *d–d* transitions above about 25 000 cm^{-1} are to levels derived from the ^3P free-ion term. However, these bands are obscured by further charge-transfer absorptions. The value of the Racah parameter *B* cannot be determined accurately and was fixed at a notional value of 850 cm^{-1}.

C.l.f. calculations (scheme CLF1) were performed for wide variations of the remaining parameters $e_\sigma(NO_2)$ and $e_{\pi\perp}(NO_2)$, and the calculated $^3B_{1g} \longrightarrow {}^3B_{2g}$ and $^3B_{1g} \longrightarrow {}^3E_g$ transition energies were compared with experiment. In the ranges $e_\sigma(NO_2)$ 1 000—5 500 and $e_{\pi\perp}(NO_2)$ −2 000 to 2 000 cm^{-1} a number of good fits were obtained but no firm conclusions about the signs or magnitudes of the nitrite c.l.f. parameters emerged. In contrast, the simultaneous fitting of the magnetic anisotropies yielded virtually unique values. The single-crystal magnetic anisotropies for $[Ni(NH_3)_4(NO_2)_2]$ have been measured down to 1.6 K although no data are reported between 300 and 80 K.[25] Moreover, at low temperatures, there is evidence for some small magnetic exchange interaction and a two-dimensional pathway for the exchange was invoked to rationalise the experimental data.[25]

The presence of substantial magnetic exchange can invalidate the assumptions used in the c.l.f. calculations. However, we observe that the relative signs of the anisotropies are maintained across the entire temperature range. Given that at 300 K the magnetic exchange has a negligible effect,[25] it follows that the *relative* values of the magnetic susceptibilities should be reliable. The c.l.f. calculations therefore concentrate on reproducing the *signs* of the anisotropies. Within the same parameter ranges as before, the magnetic data, taken with the spectra, apply

stringent constraints on the c.l.f. parameters. Qualitatively, $e_\sigma(NO_2) < e_\sigma(NH_3)$, $e_{\pi\perp}(NO_2) < 0$, $k \cong 1$, and $\zeta \cong 375$ cm^{-1}. The 'best fit' parameter values for scheme CLF1 together with calculated and observed spectroscopic and magnetic data are collected in Table 6. Note that since the CAMMAG programs cannot treat magnetic exchange effects, no attempt was made to optimise the absolute fit between observed and calculated magnetic susceptibility anisotropies.

Extension of C.L.F. Scheme.—The above scheme, CLF1, suggests $e_\sigma(NH_3) > e_\sigma(NO_2)$. For the same donor atom (here nitrogen) a correlation is expected between the magnitude of a c.l.f. e_λ parameter and the extent of λ bonding.[45] The c.l.f. analysis for $[Ni(NH_3)_4(NO_2)_2]$ therefore suggests NH_3 is a better σ donor than is NO_2^-, contrary to the *ab initio* m.o. calculations and the p.n.d. and *X*-ray diffraction results. However, the m.o. results suggested an important role for the nitrite oxygens which has not been recognised before[27] and is not included in the scheme CLF1. An Ni–O interaction can be treated explicitly by inclusion of $e_\sigma(O)$ into the parameter set as described previously for the scheme CLF2. The source of such an interaction is the oxygen lone-pair electron density. The lone pairs are some 3 Å from the metal, analogous to the axial ligands in tetragonal copper(II) complexes. In these systems, the distant, axial ligands are associated with negative e_σ values, the limit of which are the 'co-ordination voids' in truly square-planar complexes.[45] By analogy, $e_\sigma(O)$ for $[Ni(NH_3)_4(NO_2)_2]$ is expected to adopt a negative value.

Proceeding as before, $e_\sigma(NH_3)$ was set to 4 000 cm^{-1} and B to 850 cm^{-1}. The remaining parameters were varied as follows: $e_\sigma(NO_2)$ 2 500—6 000 cm^{-1}; $e_{\pi\perp}(NO_2)$ 500 to −1 000 cm^{-1}; $e_\sigma(O)$ 0 to −3 000 cm^{-1}; ζ 100—500 cm^{-1}; and k 0.5—1.0. Simultaneous fitting of the spectral and magnetic data produced some firm conclusions. First, fitting the band at 11 200 cm^{-1} shows that $e_\sigma(NO_2)$ and $e_\sigma(O)$ are correlated so that, as $e_\sigma(O)$ takes on larger, negative values, $e_\sigma(NO_2)$ adopts larger, positive values. Secondly, fitting the magnetic data indicates a modest negative value for $e_{\pi\perp}(NO_2)$; the analysis cannot support positive values for this parameter. Thirdly, ζ and k adopt similar values to those in the previous CLF1 treatment. A representative fit for scheme CLF2 is given in Table 6.

The data in Table 6 for scheme CLF2 show that the explicit recognition of a Ni–O interaction can reverse the predicted σ-donor strengths of NO_2^- and NH_3 and bring all the theoretical and experimental approaches into qualitative agreement. However, due to the correlations in the c.l.f. analysis, unique values for $e_\sigma(NO_2)$ and $e_\sigma(O)$ cannot be defined. A series of calculations analogous to the scheme CLF2 were therefore undertaken for the hexanitro species in $K_2Ba[Ni(NO_2)_6]$ to examine further the nature of Ni–NO_2 co-ordination. The site symmetry for $[Ni(NO_2)_6]^{4-}$ is nearly D_{2h}[43] so that, in the absence of oxygen interactions, the ligand-field splitting, Δ_{oct}, is as in equation (1).

$$\Delta_{oct} = 3e_\sigma(NO_2) - 2e_{\pi\perp}(NO_2) \quad (1)$$

Given the experimental Δ_{oct} value of 13 000 cm^{-1},[27] $e_\sigma(NO_2)$ is about 4 300 cm^{-1} if $e_{\pi\perp}(NO_2)$ is zero and $e_\sigma(NO_2) < 4\,300$ if $e_{\pi\perp}(NO_2) < 0$. The influence of a Ni–O interaction was investigated by adding $e_\sigma(O)$ to the parameter set and deriving an empirical function (2) expressing Δ_{oct} in terms of the three c.l.f. parameters. Both $e_\sigma(NO_2)$ and $e_\sigma(O)$ appear in equation (2)

$$\Delta_{oct} = 3e_\sigma(NO_2) - 2e_{\pi\perp}(NO_2) + 2.58e_\sigma(O) \quad (2)$$

with the same sign. In order to maintain a constant value of Δ_{oct}, these parameters must be inversely correlated so that increasing one must be compensated for by decreasing the other. The Ni–NO_2 bond length in $[Ni(NO_2)_6]^{4-}$ is shorter than in $[Ni(NH_3)_4(NO_2)_2]$ (2.08[43] against 2.15 Å[24]), hence larger e_λ magnitudes might be expected for the former compound. Assuming that $e_{\pi\perp}(NO_2) \leqslant -500$ for the hexanitrite complex {both analyses of $[Ni(NH_3)_4(NO_2)_2]$ are consistent with this bound} and substituting the experimental value for Δ_{oct} gives expression (3).

$$e_\sigma(NO_2) \leqslant 4\,000 - 0.86e_\sigma(O) \quad (3)$$

Thus, if $e_\sigma(NO_2)$ in $[Ni(NO_2)_6]^{4-}$ is to be greater than 4 000 cm^{-1}, $e_\sigma(O)$ must be negative. For $[Ni(NH_3)_4(NO_2)_2]$ with the longer Ni–NO_2 bond, the value of $e_\sigma(NO_2)$ must already be greater than the $e_\sigma(NH_3)$ value of 4 000 cm^{-1} if a consistent picture of the relative σ-donor strengths of NO_2^- and NH_3 is to be maintained. This strongly supports an $e_\sigma(NO_2)$ value in $[Ni(NO_2)_6]^{4-}$ of more than 4 000 cm^{-1} and hence a negative $e_\sigma(O)$ value. Transferring this qualitative notion of a negative $e_\sigma(O)$ back to $[Ni(NH_3)_4(NO_2)_2]$, leads to the required, larger $e_\sigma(NO_2)$ value.

Co-ordination Voids and the Nitrite Oxygen Lone Pairs.—Although the preceding argument is not conclusive, it is at least internally consistent in that negative $e_\sigma(O)$ values for *both* complexes give sensible $e_\sigma(NO_2)$ values. Moreover, the proposed negative e_σ values for the oxygen lone pairs find precedent in 'semi-co-ordinated' copper(II) complexes.[45,46] Negative e_σ values are not restricted to full co-ordination voids and a smooth progression from large positive e_σ values through to moderate negative e_σ values has been mapped out for the axial donors in a series of tetragonally elongated copper(II) amine complexes.[45]

The source of the negative sign can be traced to the c.l.f. expression (4) for an e_σ parameter,[28] where d_σ is the local

$$e_\sigma \approx \frac{|\langle d_\sigma|v|\chi_\sigma\rangle|^2}{\varepsilon_d - \bar{\varepsilon}_\chi} \quad (4)$$

σ-symmetry d orbital, of energy ε_d, in the local M–L frame, χ_σ is the local bond orbital of average energy $\bar{\varepsilon}_\chi$, and v is the local ligand-field potential. In a 'normal' M–L bond the potential, v, arises from the overlap charge density housed in χ_σ. This orbital has metal-based as well as ligand-based components such that, as the bond is stretched and the overlap charge density decreases, χ_σ tends to separate into its metal-based and ligand-based parts. The metal-based part exerts the dominant ligand-field effect for a stretched bond since it is spatially much closer to the d orbitals. For a σ interaction the appropriate metal orbital is the valence s function which is at higher energy than the basis d orbitals. Thus, the sign of the denominator in equation (4) changes and hence so does the sign of e_σ.

However, in order to produce a potential, v, the valence metal s orbital must contain some electron density.[45] The s orbital is involved with bonding to ligands elsewhere in the molecule and acquires electrons *via* this mechanism. This density is subsumed into a 'normal' M–L bond but for very long bonds and co-ordination voids the valence metal s function exerts a direct ligand-field effect. The *magnitude* of e_σ is then determined by the amount of s-electron density in χ_σ. The more that this is subsumed into bonding orbitals the less will be available for any co-ordination void interaction. Thus, in six-co-ordinate $[Ni(NH_3)_4(NO_2)_2]$, a smaller $e_\sigma(O)$ value is expected relative to a four-co-ordinate species. It might be argued that with a greater number of ligands there should be intrinsically more s-electron density and hence larger $e_\sigma(O)$ magnitudes. However, recent c.l.f. studies[46,47] have demonstrated that the total charge donation to the metal, as measured by the sum, Σ, of all the c.l.f. parameters, is approximately independent of co-ordination number, at least for metal(II) species. Given that the limiting e_σ

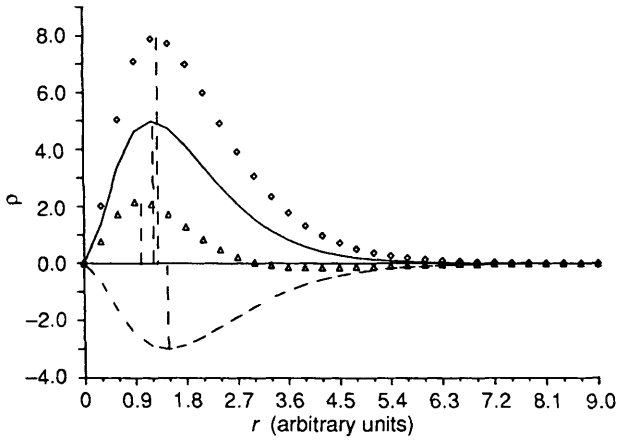

Figure 3. Schematic representation of the *d*-electron density for a nickel(II) atom using a simple r^2e^{-r} dependence. Vertical dashed lines indicate approximate maxima in density distributions; (◇) ρ(total), (△) ρ(diff), (——) ρ(↑), and (···) ρ(↓)

value for the co-ordination voids in D_{4h} $[CuCl_4]^{2-}$ is around $-3\,000$ cm^{-1},[45] with similar values suggested for planar nickel(II) and low-spin cobalt(II) complexes,[48] the value of around $-1\,200$ cm^{-1} for $e_\sigma(O)$ given in Table 6 is quite reasonable. This is associated with $e_\sigma(NO_2) = 4\,500$ cm^{-1} for $[Ni(NH_3)_4(NO_2)_2]$, implying a stronger σ donation relative to NH_3, and with an $e_\sigma(NO_2)$ value somewhat larger than 5 000 cm^{-1} for $[Ni(NO_2)_6]^{4-}$, consistent with the shorter Ni–NO_2 bond length relative to that found in $[Ni(NH_3)_4(NO_2)_2]$.

Reanalysis of P.N.D. Data.—The apparent importance of a Ni–O interaction was further investigated by reanalysing the p.n.d. data. The same model as employed previously[19] was augmented by a 1*s*-type function midway between the Ni and O atoms. The population of this 'overlap' function refined to $-0.02(1)$ without significantly affecting the other reported populations. The fit was slightly improved ($\chi = 1.58$ *versus* $\chi = 1.60$). While statistically barely significant, the non-zero Ni–O overlap population is consistent with the preceding discussion.

Another interesting facet of the p.n.d. analysis is the suggestion of an 'anti-nephelauxetic effect.'[19] The *d*-orbital radius derived from the p.n.d. experiment is *contracted* relative to the free ion. In contrast, the ubiquitous decrease, relative to their free-ion values, of the *d*–*d* interelectron repulsion parameters for metal complexes has always been interpreted as due to an *expansion* of the *d* orbitals.[49] In agreement with the latter, the DVXα calculations give an average *d*-orbital expansion (weighted according to the α- and β-spin *d* populations) of 3.5% while the *X*-ray diffraction data suggest an expansion of 1.3%. We examine whether these apparently conflicting results can be reconciled.

The analysis of the p.n.d. data used only a single set of functions to represent the spin density ρ(α) − ρ(β). The m.o. models use two sets, one for α and one for β spin. For simplicity, let us consider an isolated nickel(II) ion. Spin-polarisation effects cause a contraction of the majority (*i.e.* α) spin functions relative to the β-spin counterparts. This is most marked for the *d* orbitals where the unpaired electrons are housed. The *d*-orbital α-spin and β-spin densities, their sum, and their difference are illustrated schematically in Figure 3 for a simple r^2e^{-r} radial charge-density distribution.

The relatively contracted α-spin density, ρ(↑), dominates near the nucleus giving net positive spin there, *i.e.* ρ(diff) > 0. Further out, ρ(↑) approaches zero more rapidly than the more diffuse ρ(↓) density, even though there are more ρ(↑) electrons, leading to ρ(diff) becoming negative. Notice that the relative positions of the various maxima (the vertical dashed lines in Figure 3) indicate that ρ(diff) is *contracted* relative to *all* the other functions. Hence, if only a single radial function is used to model the spin density, it can *appear* to decrease relative to its free-ion value. This simple, semiquantitative argument explains how the *d*-orbital radius derived from the p.n.d. analysis decreases while in fact both α- and β-spin *d* orbitals expand. In addition, p.n.d. analyses often employ functions placed midway between bonded atoms to simulate overlap densities. These 'overlap' functions adopt small negative populations which correlates with the ρ(diff) < 0 region in Figure 3.

The situation depicted in Figure 3 has been further tested by combining the p.n.d. and *X*-ray populations to generate individual α- and β-spin orbital occupations. These occupations are then fixed while their separate α- and β-spin radial parameters are refined. The fit to experiment is no worse than with the restricted model (both have $\chi = 1.58$—1.60). The 'best-fit' radial parameters show that both α- and β-spin *d* orbitals expand (α by 1.3% and β by 7.1%) giving an average *d*-orbital expansion of 3.6% in remarkably good agreement with the DVXα value of 3.5%.

The above analysis incorporates many approximations and should not be taken quantitatively. Nevertheless, it does illustrate an important point concerning the care that must be taken when attempting to draw chemically useful conclusions from a least-squares procedure. Simply reproducing experimental results is not useful if the physical basis of the model is inadequate. A more rigorous treatment of the experimental data would be a simultaneous analysis of both p.n.d. and *X*-ray diffraction measurements which would allow α- and β-spin orbital populations and radii to be determined. Such a method has not yet been developed.

C.I. Effects.—Analysis of the *X*-ray diffraction data yielded a very low d_{xz} population coupled with a very high $4p_x$ population.[20] This was rationalised qualitatively[20] *via* the mixing of a doubly excited state into the ground state through c.i. In contrast to the Hartree–Fock procedure, the Hartree–Fock–Slater formalism permits non-integral m.o. occupations.[36] Hence the proposed c.i. interaction might be investigated, albeit in an *ad hoc* way, by using the transition-state procedure.[36] The formal equivalence between the electron density computed *via* non-integral m.o. occupations (*i.e.* Slater's transition-state formalism) and that from a c.i. treatment can be easily demonstrated (Appendix). However, unlike the c.i. scheme, the transition-state method provides no well defined, unique way of choosing the m.o. occupation numbers. Nevertheless, by removing equal amounts of α- and β-spin density from the mainly $3d_{xz}$ ($3b_{2g}$) m.o.s and placing this into the mainly $4p_x$ m.o.s, the subsequent relaxation of the electron density as the calculation is converged could, in principle, provide some insight into the plausibility of the proposed c.i. mechanism.

There is no single m.o. dominated by the $4p_x$ orbital. Rather it is shared almost equally between the $9b_{3u}$ and $10b_{3u}$ functions, with the remaining parts consisting of H 1*s* orbitals. The DVXα s.c.c. calculations therefore suggest a more complicated c.i. interaction than the simple mechanism proposed above. In an attempt to model the simpler interaction, albeit partially, a calculation was performed in which a total of 0.5 electron (0.25 α + 0.25 β) was transferred from the $3b_{2g}$ levels to the $9b_{3u}$ m.o.s. The resulting relaxed orbital populations are roughly what could have been inferred simply from the ground-state m.o. compositions (Table 4). Relaxation affects mainly the d_{z^2} orbital, where the total charge increases fairly rapidly (from 1.31 to 1.52) while the spin population drops (from 0.68 to 0.42). Apart from this, the charge populations appear to approach

experiment more closely but the spin populations are less satisfactory. Perhaps a more accurate DVXα calculation, using a better description of the molecular potential,[50] may yield more suitable 4*p*-type functions, but a rigorous c.i. treatment appears to be called for.

Conclusion

A careful analysis of *ab initio* UHF and DVXα m.o. calculations, c.l.f. results, and experimental diffraction data for $[Ni(NH_3)_4(NO_2)_2]$ has led to a consistent picture of the electronic structure and M–L bonding in this complex. The nitrite ligand acts as a better σ donor than does ammonia. The NH_3 molecules show no tendency to π bonding while NO_2^- displays a weak π interaction of uncertain sign perpendicular to the ligand plane. The m.o. calculations suggest a significant interaction parallel to the NO_2 plane arising from the oxygen atoms. Explicit recognition of this Ni–O interaction is required to bring the c.l.f. description of the bonding in $[Ni(NH_3)_4(NO_2)_2]$ into qualitative agreement with the m.o. calculations and diffraction results. A reanalysis of the p.n.d. data is also consistent with this effect.

Although the qualitative reproduction of the experimental data is satisfactory, there remain significant quantitative discrepancies. Some of these problems have been ascribed to c.i. effects which were modelled in an *ad hoc* way *via* DVXα transition-state calculations. The theoretical results were inconclusive indicating the need for a rigorous c.i. treatment. However, other anomalies, such as the 'anti-nephelauxetic effect,' proposed to explain the apparent contraction of the *d* orbitals used to model the p.n.d. data, can be traced to the inadequate flexibility of the least-squares modelling procedure. A better scheme would be to treat simultaneously both p.n.d. and *X*-ray diffraction data sets. Moreover, given the differences between theoretical Mulliken populations and experimental multipole populations, future studies would be better based on a direct comparison of computed and observed experimental data such as structure factors. The development of such a procedure provides an important challenge for the future.

Appendix

Densities from Fractional Occupation of Orbitals and from C.I. Expansions.—The formal equivalence of the calculated electron density using non-integral m.o. occupation numbers (Slater's transition state formalism) and mixed configurations (c.i.) can be shown as follows.

In a single determinantal approximation with all m.o.s orthogonal, expression (A1) can be written where n_i is the

$$\rho(\vec{r}) = \Sigma_i n_i \varphi_i^*(\vec{r})\varphi_i(\vec{r}) \qquad \text{(A1)}$$

occupation of each orbital and φ_i is an m.o. For example, the determinant, ψ, for the ground state of H_2 is given by $\psi = \frac{1}{2}|\sigma_g\bar{\sigma}_g|$.

Suppose we choose to examine the case where the σ_u orbitals are each occupied by $\frac{1}{2}$ an electron, *i.e.* $\psi_{\frac{1}{2}} = 1/\sqrt{4!}|\sigma_g^{\frac{1}{2}}\bar{\sigma}_g^{\frac{1}{2}}\sigma_u^{\frac{1}{2}}\bar{\sigma}_u^{\frac{1}{2}}|$ and expression (A2) is obtained. The same density

$$\rho(r) = \tfrac{1}{2}(\sigma_g^2 + \bar{\sigma}_g^2 + \sigma_u^2 + \bar{\sigma}_u^2) = \sigma_g^2 + \sigma_u^2 \qquad \text{(A2)}$$

would be obtained by a c.i. calculation which involved equal mixing of the σ_g^2 and σ_u^2 configurations of H_2, *i.e.* $\psi_{c.i.} = 1/\sqrt{2}\{|\sigma_g\bar{\sigma}_g| + |\sigma_u\bar{\sigma}_u|\}$.

The density operator $\Sigma_i\delta(R - r_i)$ is a one-electron operator, so for double excitations there will be no matrix elements between different determinants. Hence equation (A3) is

$$\rho(\vec{r}) = \Sigma_i n_i \varphi_i^*(\vec{r})\varphi_i(\vec{r}) \qquad \text{(A3)}$$

obtained for each of the determinants in the expansion. For $\psi_{c.i.}$ this becomes $\frac{1}{2}(\sigma_g^2 + \bar{\sigma}_g^2 + \sigma_u^2 + \bar{\sigma}_u^2) = \sigma_g^2 + \sigma_u^2$.

Acknowledgements

R. J. D. acknowledges the award of an Australian National Research Fellowship.

References

1 B. N. Figgis and P. A. Reynolds, *Int. Rev. Phys. Chem.*, 1986, **5**, 265.
2 B. N. Figgis, E. S. Kucharski, and P. A. Reynolds, *Acta Crystallogr., Sect. B*, 1989, **45**, 240.
3 See C. W. Bauschlicher, S. P. Walch, and S. R. Langhof, in 'Quantum Chemistry: The Challenge of Transition Metals and Coordination Chemistry,' NATO ASI Series C, vol. 176, pp. 15–37, ed. A. Veillard, Reidel, Dordrecht, 1986.
4 H. Johansen and N. K. Andersen, *Mol. Phys.*, 1986, **58**, 965.
5 P. W. Fowler and N. C. Pyper, *Proc. R. Soc. London, Ser. A*, 1985, **398**, 377.
6 V. Luana, M. Bermejo, M. Florez, J. M. Recio, and L. Pueyo, *J. Chem. Phys.*, 1989, **90**, 6409.
7 P. Day, *J. Phys. (Paris)*, 1982, **C7**, 341.
8 B. N. Figgis, P. A. Reynolds, and G. A. Williams, *J. Chem. Soc., Dalton Trans.*, 1980, 2339.
9 B. N. Figgis, R. Mason, A. R. P. Smith, and G. A. Williams, *J. Am. Chem. Soc.*, 1979, **101**, 3673.
10 B. N. Figgis, P. A. Reynolds, and G. A. Williams, *J. Chem. Soc., Dalton Trans.*, 1980, 2348.
11 B. N. Figgis, G. A. Williams, J. B. Forsyth, and R. Mason, *J. Chem. Soc., Dalton Trans.*, 1981, 1837.
12 B. N. Figgis, P. A. Reynolds, and R. Mason, *Inorg. Chem.*, 1984, **23**, 1149.
13 B. N. Figgis, J. B. Forsyth, and P. A. Reynolds, *Inorg. Chem.*, 1987, **26**, 101.
14 G. S. Chandler and R. A. Phillips, *J. Chem. Soc., Faraday Trans. 2*, 1986, 573.
15 G. S. Chandler and R. A. Phillips, *J. Chem. Soc., Faraday Trans. 2*, submitted for publication.
16 G. S. Chandler, B. N. Figgis, R. A. Phillips, P. A. Reynolds, and R. Mason, *J. Phys. (Paris)*, 1982, **C7**, 323.
17 R. J. Deeth, B. N. Figgis, and M. I. Ogden, *Chem. Phys.*, 1988, **121**, 115.
18 D. E. Ellis and G. S. Painter, *Phys. Rev. B*, 1970, **2**, 2887.
19 B. N. Figgis, P. A. Reynolds, and R. Mason, *J. Am. Chem. Soc.*, 1983, **105**, 440.
20 B. N. Figgis, P. A. Reynolds, and S. Wright, *J. Am. Chem. Soc.*, 1983, **105**, 434.
21 C. R. Hare and C. J. Ballhausen, *J. Chem. Phys.*, 1964, **40**, 792.
22 I. Bertini, D. Gatteschi, and A. Scozzafava, *Inorg. Chem.*, 1976, **15**, 203.
23 B. J. Kennedy, K. S. Murray, M. A. Hitchman, and G. L. Rowbottom, *J. Chem. Soc., Dalton Trans.*, 1987, 825.
24 B. N. Figgis, P. A. Reynolds, A. H. White, G. A. Williams, and S. Wright, *J. Chem. Soc., Dalton Trans.*, 1981, 997.
25 B. N. Figgis, B. J. Kennedy, K. S. Murray, P. A. Reynolds, and S. Wright, *Aust. J. Chem.*, 1982, **35**, 1807.
26 A. B. P. Lever, I. M. Walker, P. J. McCarthy, K. B. Mertes, A. Jircitano, and R. Sheldon, *Inorg. Chem.*, 1983, **22**, 2252.
27 M. A. Hitchman and G. L. Rowbottom, *Coord. Chem. Rev.*, 1982, **42**, 55.
28 M. Gerloch, J. H. Harding, and R. G. Woolley, *Struct. Bonding (Berlin)*, 1981, **46**, 1.
29 B. N. Figgis, P. A. Reynolds, G. A. Williams, and N. Lehner, *Aust. J. Chem.*, 1981, **34**, 993.
30 D. Goutier, R. Macaulay, and A. J. Duke, 'Quantum Chemistry Program Exchange,' Indiana University, 1974, vol. 10, p. 241.
31 B. Roos, A. Veillard, and G. Vinot, *Theoret. Chim. Acta*, 1971, **20**, 1.
32 A. J. H. Wachters, *J. Chem. Phys.*, 1970, **52**, 1033.
33 D. M. Hood, R. M. Pitzter, and H. F. Schaeffer III, *J. Chem. Phys.*, 1979, **71**, 705.
34 K. Rudenberg, R. C. Raffinetti, and R. D. Bardo, 'Energy Structure and Reactivity,' eds. D. W. Smith and W. B. McKae, Wiley, New York, 1973.

35 F. B. van Diujneveldt, IBM Research Report RJ 945, San Jose, California, 1971.
36 J. C. Slater, 'Quantum Theory of Molecules and Solids,' McGraw-Hill, New York, 1974, vol. 4.
37 E. J. Baerends, D. E. Ellis, and P. Ros, *Chem. Phys.*, 1973, **2**, 41.
38 E. J. Baerends and P. Ros, *Chem. Phys.*, 1973, **2**, 52.
39 F. W. Averill and D. E. Ellis, *J. Chem. Phys.*, 1973, **59**, 6412.
40 E. J. Baerends, D. E. Ellis, and P. Ros, *Theoret. Chim. Acta*, 1972, **27**, 339.
41 M. Gerloch, 'Magnetism and Ligand Field Analysis,' Cambridge University Press, New York, 1983.
42 CAMMAG, a FORTRAN program by D. A. Cruse, J. E. Davies, M. Gerloch, J. H. Harding, D. J. Mackey, and R. F. McMeeking, University of Cambridge, 1975.
43 S. Takagi, M. D. Joester, and P. G. Lenhert, *Acta Crystallogr., Sect. B*, 1975, **31**, 1970.
44 D. E. Ellis, personal communication.
45 R. J. Deeth and M. Gerloch, *Inorg. Chem.*, 1984, **23**, 3846.
46 R. J. Deeth and M. Gerloch, *Inorg. Chem.*, 1985, **24**, 1754.
47 R. J. Deeth and M. Gerloch, *Inorg. Chem.*, 1985, **24**, 4490.
48 M. A. Hitchman and J. B. Bremner, *Inorg. Chim. Acta*, 1978, **27**, L61.
49 C. J. Ballhausen, 'Introduction to Ligand Field Theory,' McGraw-Hill, New York, 1962.
50 B. Delley and D. E. Ellis, *J. Chem. Phys.*, 1982, **76**, 1949.

Received 20*th October* 1989; *Paper* 9/04528G